THE JOURNAL OF PHYSICAL CHEMISTRY B

Article

pubs.acs.org/JPCB

Adsorption of Sodium Dodecyl Sulfate on Functionalized Graphene Measured by Conductometric Titration

Andrew G. Hsieh,[†] Christian Punckt,[†,‡] Sibel Korkut,[†,‡] and Ilhan A. Aksay*[,†]

[†]Department of Chemical and Biological Engineering, Princeton University, Princeton, New Jersey 08544, United States

[‡]Vorbeck Princeton Research Center, Vorbeck Materials Corp., 11 Deerpark Drive, Monmouth Junction, New Jersey 08852, United States

ABSTRACT: We report on the adsorption of sodium dodecyl sulfate (SDS) onto functionalized graphene sheets (FGSs) in an aqueous system, measured at broad SDS and FGS concentration ranges by conductometric surfactant titration. At dilute SDS concentrations (<12 μM in bulk solution), there is evidence of a counterion exchange between hydronium ions (from the dissociation of acidic chemical functionalities on FGS) and sodium ions coadsorbing with dodecyl sulfate monomers onto FGSs. We find that, for FGS with a carbon-to-oxygen ratio of ~18, monolayer adsorption of SDS on FGS reaches full surface coverage by ~12 μM SDS. Additionally, the critical surface aggregation concentration (csac) for surface micelle formation on FGS is measured to be ~1.5 mM SDS. The transition from monolayer adsorption to surface micelle formation appears to occur at a similar SDS concentration on FGSs as on graphite, suggesting there is little difference in the surfactant adsorption behavior on both materials. We estimate that the FGS surface area available for SDS adsorption is ~600 m^2/g, which is significantly less than expected for FGSs in suspension and indicates the presence of regions on FGS on which SDS adsorption does not occur.

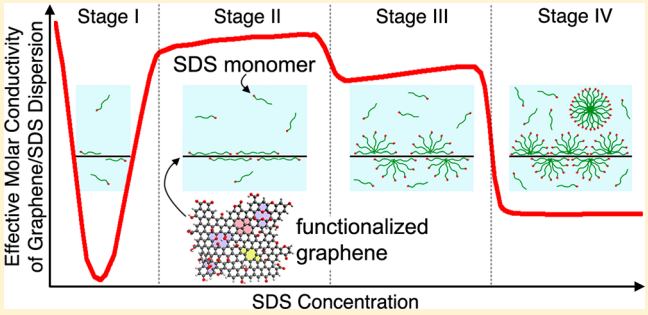

INTRODUCTION

Functionalized graphene sheets (FGSs), which can be produced in large quantities by thermal exfoliation and reduction of graphite oxide (GO)[1,2] or by chemical reduction of graphene oxide,[3] have been used to improve performance in many applications, including graphene-metal oxide nanocomposites for Li-ion battery electrodes,[4,5] graphene-polymer composites,[6−8] and high surface area tapes.[9] While surfactant adsorption plays a key role in these applications, e.g., as a dispersant to obtain aqueous FGS suspensions[10,11] or as a template for the growth of metal oxide films,[12,13] the adsorption behavior of surfactants on functionalized graphene has not been studied in detail.

On the other hand, surfactant adsorption onto graphitic carbons has been investigated extensively: Evidence from molecular dynamics simulations[14−16] and calorimetry[17−19] indicates that surfactant molecules initially, i.e., at small concentrations, adsorb with their alkyl chains oriented parallel to the basal plane of graphite, eventually forming a monolayer via a coexistence between surfactant-rich and surfactant-lean regions.[14,18,19] At the critical surface aggregation concentration (csac), a transition to the formation of hemicylindrical micelles on the substrate occurs.[20,21] As the surfactant concentration is increased beyond the csac, the surface micelles increase in number density and are aggregated, as seen with direct imaging of micelles adsorbed on highly oriented pyrolytic graphite (HOPG) using liquid-cell atomic force microscopy (AFM).[22−24] The orientation of surface micelles is influenced mainly by the underlying crystal structure[25,26] as well as by topographical steps and ledges on the substrate.[26] Upon further increase of the surfactant concentration, the spacing between surface micelles decreases until the surface is saturated.[27] Adsorption isotherms for ionic alkyl surfactants on graphitic carbons therefore typically display a two-step adsorption behavior,[21,28,29] reflecting an initial period of monolayer formation at low surfactant concentrations (below the csac), followed by the formation and subsequent "densification" of surface micelles.

Compared to the basal plane of graphite (i.e., pristine graphene), in which carbon atoms are predominantly sp^2 hybridized and exhibit a high degree of hexagonal order, the structure of FGS is highly disordered due to the presence of lattice defects (topological defects and vacancies)[30,31] as well as oxygen-containing chemical functionalities (Figure 1).[1,31,32] As such, surfactants may not exhibit the same adsorption behavior on functionalized graphene as they do on pristine graphene. However, to date, very little information about surfactant adsorption on FGSs is available in the literature. In a recent experimental study, Glover et al. used liquid-cell AFM to directly image graphene oxide and FGS (produced via thermal

Received: April 18, 2013
Revised: June 3, 2013
Published: June 4, 2013

   dx.doi.org/10.1021/jp403876t | J. Phys. Chem. B 2013, 117, 7950−7958

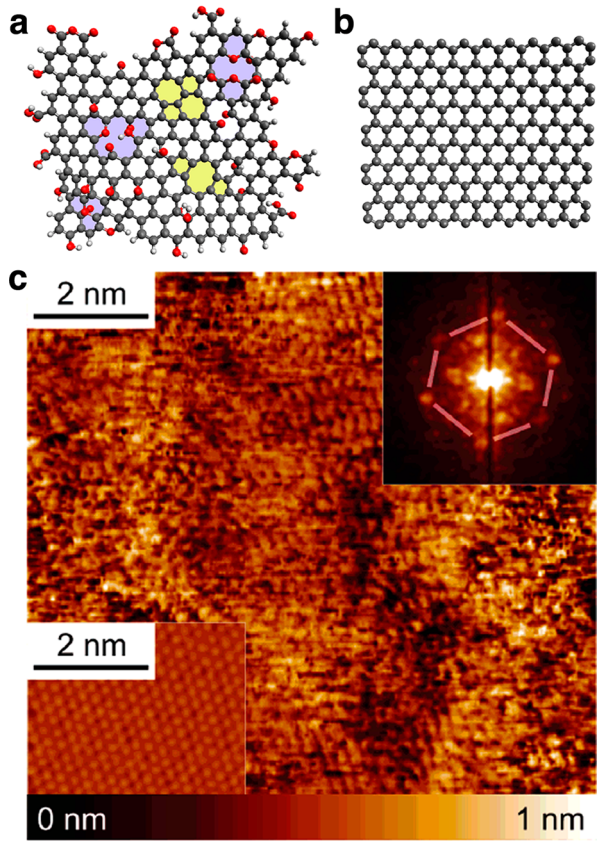

Figure 1. (a) Schematic of a functionalized graphene sheet (FGS), showing carbon (gray), hydrogen (white), and oxygen atoms (red) as well as 5−8−5 and 5−7−7−5 topological defects (yellow) and lattice vacancies (blue). (b) Schematic of the basal plane of graphite (i.e., pristine graphene). (c) Scanning tunneling microscopy (STM) topography image of FGS demonstrating the highly disordered structure, taken at a bias voltage of 30 mV and a current of 5 nA; the Fourier transform (inset, top right) shows that hexagonal order is still present in FGSs. The bottom left inset shows an STM image of HOPG, taken under identical conditions with the same topography color map as the main image, showing the high degree of hexagonal order (reprinted with permission from ref 30; Copyright American Chemical Society, 2006).[30]

exfoliation and reduction of graphite oxide) on an HOPG substrate immersed in an aqueous surfactant solution[33] and demonstrated that at a surfactant concentration above the critical micelle concentration (cmc), i.e., where micelles are present in bulk solution,[34,35] the amount of surfactant that can adsorb onto graphene depends strongly on the degree of graphene oxidation. While only a single surfactant concentration was considered, this study illustrates that the lattice defects[30,31] and oxygen-containing functional groups[1,31,32] exhibited by FGSs alter the surfactant adsorption behavior on FGSs as compared to graphite or even pristine graphene (in which carbon atoms are also predominantly sp^2 hybridized and arranged in a hexagonal lattice). In the work presented herein, using the anionic surfactant sodium dodecyl sulfate (SDS), we aim to determine if the adsorption of surfactants on FGSs displays a two-step behavior as on graphitic carbons and also if the csac occurs at a similar concentration.

Many techniques have been used to study surfactant adsorption at solid−liquid interfaces, such as two-phase dye extraction,[28] calorimetry,[17−19] ion-selective electrodes,[21] STM,[36−38] and liquid-cell AFM.[23,26,33] However, conductometric surfactant titration is unique in its ability to sample a broad range of concentrations with high resolution. In this technique, the conductivity of a sample suspension or solution is measured while it is titrated with a surfactant solution. The conductivity λ of deionized (DI) water as a function of SDS concentration is well documented.[39−42] Following Kohlrausch's law of independent ion migration,[43,44] λ of an SDS solution can be written as a function of the concentrations of the ionic species in the system[40]

$$\lambda = \lambda_0 + \Lambda_0^{Na+}[Na^+]_{bulk} + \Lambda_0^{DS-}[DS^-]_{bulk} + \left(\Lambda_0^{Na+}\beta + \frac{\Lambda_0^{mic}}{N}\right)[DS^-]_{mic} \quad (1)$$

where λ_0 is the initial solvent conductivity, $[DS^-]_{bulk}$ and $[Na^+]_{bulk}$ are the concentrations of free dodecyl sulfate (DS^-) monomers and sodium (Na^+) counterions in bulk solution, and $[DS^-]_{mic}$ represents the DS^- that are part of ionic micelles, expressed as the equivalent concentration that would be obtained if the DS^- were monomers in solution. Λ_0^{Na+}, Λ_0^{DS-}, and Λ_0^{mic} are the molar conductivities of Na^+, DS^-, and micelles, respectively. N is the aggregation number (average number of DS^- per micelle) and β is the degree of dissociation of micelles (fraction of SDS within micelles that is dissociated). In good agreement with experiments, eq 1 predicts a linear increase in λ with SDS concentration, with a decrease in the slope when micelle formation begins to dominate at the cmc.[34,35]

When particles are introduced to the surfactant solution, a fraction of the surfactant molecules may adsorb onto the particles. This changes the concentration of ionic species in the bulk solution, which in turn influences the overall conductivity of the system. The surfactant adsorption behavior can then be determined by analyzing the differences in conductivity between titrations of DI water and the particle suspension. In this study, we use conductometric titration to determine the adsorption behavior of SDS onto FGSs in a wide range of surfactant concentrations. We observe a counterion exchange during the initial stages of monolayer adsorption and identify the bulk SDS concentration by which the adsorbed SDS monolayer reaches full surface coverage. In addition, we measure the csac for SDS surface micelle formation on FGSs, and we contend that the transition from monolayer adsorption to surface micelle formation occurs at a similar SDS concentration on FGSs as on graphitic carbon. This suggests that there is little difference in the apparent surfactant adsorption behavior on both materials. Furthermore, our estimation of the FGS surface area available for SDS adsorption is significantly less than expected for functionalized graphene in suspension, which indicates that there are regions on FGS on which SDS adsorption does not occur.

METHODS

Production of FGSs. GO was prepared according to the Staudenmaier method,[45] and as further detailed in more recent publications.[1,2] The GO was placed at the bottom of a fused silica tube (Technical Glass Products) and dried overnight under a flow of nitrogen. The tube was then evacuated and purged with ultrahigh purity argon (Air Products), and the simultaneous thermal reduction and exfoliation of GO was carried out at 1100 °C under vacuum in a three-zone tube furnace (Lindberg/Blue M, SPX Thermal Product Solutions). The as-produced dry FGS powder had a surface area of

dx.doi.org/10.1021/jp403876t | J. Phys. Chem. B 2013, 117, 7950−7958

~690 m^2/g, determined from nitrogen adsorption data (Gemini V, Micrometrics Instruments Corporation) by the Brunauer, Emmett, and Teller (BET) method.[46] The molar carbon-to-oxygen ratio (C/O) of the as-produced FGS powder was ~18, measured by energy dispersive X-ray spectroscopy (INCA x-act, Oxford Instruments, attached to a Vega 1 scanning electron microscope from Tescan).

Conductometric Surfactant Titration. SDS stock solutions with concentrations of 2, 10, and 100 mM were prepared by dissolving SDS (Sigma Aldrich, ≥99% purity, used as received) in DI water (Picopure 2 UV Plus system, Hydro Service and Supplies, Inc.). Aqueous stock suspensions of FGSs were prepared by first sonicating the FGSs in ethanol (VCX 750 ultrasonic processor unit, Sonics & Materials, Inc.) to obtain a dispersion of the as-prepared material. Then, using dialysis membranes (Spectra/Por 7, MWCO 15 kD), a solvent exchange was carried out for one week in a water bath that was refreshed daily in order to remove the ethanol as well as any other water-soluble impurities. The FGS stock suspensions typically had a final FGS concentration of ~1.2−1.4 mg/mL, and were then diluted with DI water to obtain 100 mL samples with FGS concentrations ranging from 0.01 to 1 mg/mL. All the solutions and suspensions were allowed to equilibrate in air for 1 h before the experiments were started in order to eliminate changes in conductivity caused by the uptake of atmospheric CO_2.

Conductometric titration was carried out by adding SDS solution to an FGS suspension at a rate of 6 mL/h using a syringe pump (Harvard Apparatus). To obtain high-resolution data within a wide range of surfactant concentrations (from 0.01 to over 10 mM), separate titrations were carried out using each of the 2, 10, and, 100 mM SDS stock solutions. The FGS suspension was contained in a jacketed beaker to maintain a constant temperature of 25 °C, continuously stirred, and subjected to 5 s ultrasound pulses every 15 s. A conductivity meter (CDM83, Radiometer Copenhagen) with a temperature compensation probe was used to measure the conductivity, and data points were collected in between ultrasound pulses, i.e., in the absence of ultrasonic agitation.

RESULTS AND DISCUSSION

Figure 2a shows the conductivity λ of both DI water and a 0.5 mg/mL aqueous FGS suspension during titrations with SDS, as a function of the amount of SDS added to the system. The amount of added surfactant is expressed as the equivalent concentration $[SDS]_{eq}$ that would be obtained if all the SDS in the system were dissolved in DI water. To better visualize changes in the slope of the conductivity, we plot the effective molar conductivity $\lambda' = (d\lambda)/(d[SDS]_{eq})$ in Figure 2b. In the insets of Figure 2, we provide higher resolution sections of λ and λ' in the range up to $[SDS]_{eq}$ = 1 mM. The differences in λ and λ' between the titration of water and the titration of the FGS suspension are indicative of SDS adsorption onto FGSs. To understand the underlying physical processes, we first analyze the conductivity behavior of the water titration to validate our approach and then analyze the conductivity behavior of the FGS suspension.

Conductometric Titration of Water. The conductivity of aqueous SDS solutions is well documented, and the plots of λ and λ' in Figure 2 for the titration of water with SDS are in good agreement with the literature.[39−42] For DI water, λ is initially ~1 $\mu S \cdot cm^{-1}$ and the pH is ~5.7, which is a result of dissolved atmospheric CO_2 forming a small amount of carbonic acid.[47] As SDS is added, λ increases monotonically with $[SDS]_{eq}$ up to ~7 mM while λ' decreases slightly from 70 to 64 $mS \cdot cm^{-1}M^{-1}$. Upon further addition of SDS, λ transitions to a lower slope regime, with λ' dropping from 64 $mS \cdot cm^{-1}M^{-1}$ at 7 mM to 26 $mS \cdot cm^{-1}M^{-1}$ at 10 mM. This decrease in λ' is indicative of a micelle aggregation transition for SDS in bulk solution.[48] Based on the model developed by Phillips, which assumes that only the surfactant monomer and micelle concentrations influence the property of interest (λ in our case),[49] the cmc is taken as the inflection point in λ', which we observe at ~8 mM. This agrees with literature values of the cmc for SDS in water, which range from 8.0 to 8.4 mM.[39,41,50,51] Above the aggregation transition, λ increases monotonically with $[SDS]_{eq}$ while λ' decreases to 25 $mS \cdot cm^{-1}M^{-1}$ at 14 mM SDS.

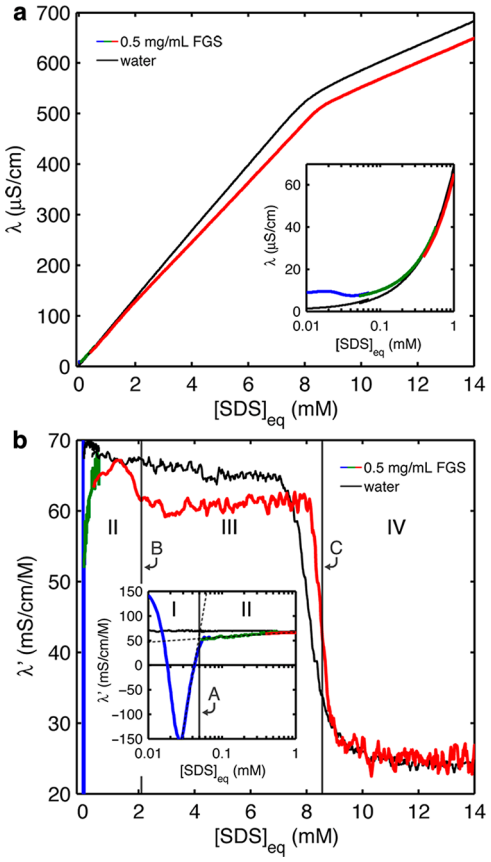

Figure 2. (a) Conductivity, λ, of a 0.5 mg/mL FGS suspension, measured from three separate titrations that used SDS solutions with concentrations of 2 mM (blue), 10 mM (green), and 100 mM (red) in order to obtain high-resolution data within a wide range of surfactant concentrations; also shown is λ of DI water (black) that was titrated with SDS solutions using the same three concentrations. (b) The derivative of conductivity, λ', calculated with respect to the SDS equivalent concentration in the system, $[SDS]_{eq}$, for both the FGS suspension and DI water. The indicated stages I−IV are discussed in the text.

These observations can be understood by considering that, at concentrations below the cmc, surfactant molecules fully dissociate into DS^- monomers and Na^+ counterions.[34,35] Thus, as $[Na^+]_{bulk} = [DS^-]_{bulk}$ and $[DS^-]_{mic}$ is zero, eq 1 shows that the slope of λ below the cmc is the sum of Λ_0^{Na+} and Λ_0^{DS} (see Appendix A for details). The slight decrease observed in λ' below the cmc is in agreement with Kohlrausch's foundational work on the conductivity of strong electro-

dx.doi.org/10.1021/jp403876t | J. Phys. Chem. B 2013, 117, 7950−7958

lytes:[43,44,52] At the limit of infinite dilution, the molar conductivity of an electrolyte is the highest; however, as the electrolyte concentration increases, the ions begin to interact, causing a decrease in their mobility[43,44] and activity coefficient,[53,54] which consequently decreases the molar conductivity. During the micelle aggregation transition, the added surfactant molecules begin to form micelles with an average aggregation number of N, which increases in value with $[SDS]_{eq}$.[34] The sharpness of this transition (i.e., the span of the λ' decrease) is determined by the width of the micelle size distribution, by how rapidly N increases with $[SDS]_{eq}$, and by the magnitude of N when it stabilizes in value.[48] Above the transition, further additions of surfactant molecules do not increase N appreciably, but rather increase the overall number density of micelles,[35,55] resulting in an increase in $[DS^-]_{mic}$ and in the concentration of Na^+ dissociated from micelles $[Na^+]_{mic}$. This causes λ to grow at a rate dominated by the molar conductivity of micelles and the fraction of sodium ions that dissociate from them. As micelles are only partially dissociated,[55−58] the DS^- in micelles exhibit a significantly smaller molar conductivity compared to free DS^- monomers. The growing ionic strength causes $[DS^-]_{bulk}$ and $[Na^+]_{bulk}$ to decrease as $[SDS]_{eq}$ increases above the cmc,[59,60] which in turn influences the value of λ'. However in the range of $[SDS]_{eq}$ examined herein, this effect is small. In addition, our focus is on the behavior of λ and λ' below the cmc. Nevertheless, understanding the influence of $[SDS]_{eq}$ on λ' above the cmc may be the subject of a future study. An in-depth discussion of Figure 2 and the validation of eq 1 for the titration of water with SDS are provided in Appendix A.

Conductometric Titration of Aqueous FGS Suspensions. When FGSs are introduced to an SDS solution, a dynamic equilibrium is established between DS^- adsorbing onto FGSs and DS^- remaining in bulk solution. The amount of DS^- adsorbed onto FGSs can be expressed as the equivalent concentration $[DS^-]_{ads}$ that would be obtained if the adsorbed DS^- were dissolved in water. This yields $[DS^-]_{bulk} = [SDS]_{eq} - [DS^-]_{ads}$ and $[Na^+]_{bulk} = [SDS]_{eq} - (1 - \beta^*)[DS^-]_{ads}$, where β^* is the degree of dissociation of adsorbed DS^-, such that $[Na^+]_{ads} = (1 - \beta^*)[DS^-]_{ads}$. Below the cmc, λ as a function of $[SDS]_{eq}$ can thus be written as

$$\lambda = \lambda_0 + (\Lambda_0^{Na+} + \Lambda_0^{DS-})[SDS]_{eq} - (\Lambda_0^{Na+}(1 - \beta^*) + \Lambda_0^{DS-})[DS^-]_{ads} \quad (2)$$

Here, an additional term of the form $\Lambda_0^{FGS}\,\beta^*\,[DS^-]_{ads}$ may be included to reflect the conductivity resulting from the diffusion of FGSs with adsorbed DS^-. However, the contribution of these charged particles to the overall suspension conductivity is several orders of magnitude smaller than the contribution of Na^+, DS^-, and ionic micelles (see Appendix B). We therefore neglect the contribution of FGS migration to conductivity. The expression for λ', then, is

$$\lambda' = \frac{d\lambda}{d[SDS]_{eq}} = (\Lambda_0^{Na+} + \Lambda_0^{DS-}) - (\Lambda_0^{Na+}(1 - \beta^*) + \Lambda_0^{DS-})\left(\frac{d[DS^-]_{ads}}{d[SDS]_{eq}}\right) \quad (3)$$

From eq 3, due to the adsorption of SDS on FGSs, we expect λ' to be non-negative and less than or equal to λ' from the titration of water. Additionally, we see from the second term in eq 3 that, as $[SDS]_{eq}$ increases, λ' should decrease if an increasing fraction of the added SDS adsorbs onto FGSs, consequently leaving a smaller fraction of the added SDS in bulk solution to conduct electricity. It should be noted that β^* is likely not constant but decreases with increasing $[DS^-]_{ads}$, in particular, when approaching the csac.[15] Therefore, a decrease in λ' may also be associated with a decrease in the degree of dissociation of adsorbed surfactant.

As shown in Figure 2, we observe a significantly different conductivity behavior for the titration of a 0.5 mg/mL aqueous FGS suspension than for the titration of water. During our analysis of the FGS suspension titration, we divide λ' into four stages (as indicated in Figure 2b). Stage I starts at the beginning of the titration, where we measure an initial conductivity of 10 $\mu S \cdot cm^{-1}$ as well as a suspension pH of ∼4.5, which is lower than for water in equilibrium with air.[47] We attribute this pH difference to the dissociation of acidic functional groups on FGSs,[1,30] which also gives rise to the higher initial λ compared to DI water. Upon the addition of SDS, λ initially increases at twice the rate of the water titration ($\lambda' \approx 140$ $mS \cdot cm^{-1}M^{-1}$ as compared to 70 $mS \cdot cm^{-1}M^{-1}$). As more SDS is added, λ continues to increase; however, λ' decreases steadily and reaches a value of 0 $mS \cdot cm^{-1}M^{-1}$ at $[SDS]_{eq} \approx 18$ μM. At this point, λ' becomes negative and continues to decrease until $[SDS]_{eq} \approx 27$ μM, above which λ' increases and reaches a value of 0 $mS \cdot cm^{-1}M^{-1}$ at $[SDS]_{eq} \approx 43$ μM. The negative values of λ' reflect the decrease in λ between the local maximum and minimum observed in the inset of Figure 2a. Upon further addition of SDS, λ increases monotonically with $[SDS]_{eq}$ as in the water titration; however, λ' has a more complex behavior, increasing to ∼50 $mS \cdot cm^{-1}M^{-1}$ at $[SDS]_{eq} \approx 54$ μM and then leveling off.

As discussed in the determination of the cmc in the previous subsection, there is a fundamental basis for using inflection points in λ' to determine transitions in surfactant behavior, as proposed by Phillips.[49] However, in Stage I, the initially high values of λ' compared to the water titration and the subsequent negative values of λ' complicate the application of Phillips' approach. To circumvent this complication, based on the forthcoming physical interpretation, we allow the leveling-off behavior to mark the transition between Stages I and II of the titration, and thus we define the boundary between the stages (line A) as the intersection of the linear extrapolations of λ' before and after leveling off, as indicated in the inset of Figure 2b.

In Stage II of the titration, λ' increases gradually to ∼67 $mS \cdot cm^{-1}M^{-1}$ at $[SDS]_{eq} \approx 1.3$ mM. At this point, λ' decreases and reaches a value of ∼59 $mS \cdot cm^{-1}M^{-1}$ at $[SDS]_{eq} \approx 3$ mM. The inflection point of this decrease (line B) marks the transition to Stage III, in which λ' gradually increases to ∼62 $mS \cdot cm^{-1}M^{-1}$ at $[SDS]_{eq} \approx 8$ mM. This is followed by a decrease in λ' to ∼26 $mS \cdot cm^{-1}M^{-1}$ at $[SDS]_{eq} \approx 10$ mM. The inflection point of this decrease occurs at ∼8.5 mM (line C) and marks the transition to Stage IV, in which λ' maintains a value of ∼26 $mS \cdot cm^{-1}M^{-1}$ as $[SDS]_{eq}$ increases further. This matches, within error, the value of λ' above the cmc in the titration of water.

Conductometric titration was carried out at a range of FGS concentrations, and λ' qualitatively exhibited the same behavior, displaying all four stages as described above and shown in Figure 2b, except in the 0.01 and 0.05 mg/mL suspensions at the transitions from Stages I to III and in the 0.1 mg/mL suspension between Stages II and III, as the

dx.doi.org/10.1021/jp403876t | J. Phys. Chem. B 2013, 117, 7950−7958

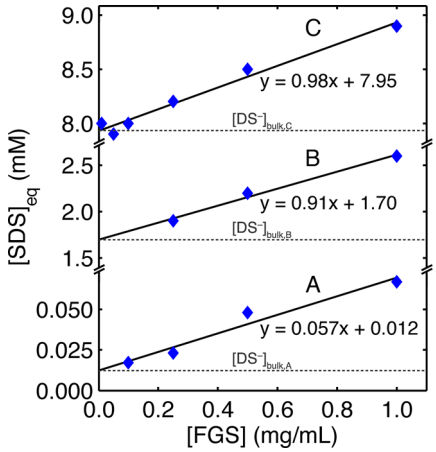

Figure 3. SDS equivalent concentrations, $[SDS]_{eq}$, at which the boundaries between Stages I and II (line A), Stages II and III (line B), and Stages III and IV (line C) occur during conductometric titrations of aqueous FGS suspensions with solutions of SDS, as a function of the concentration of FGSs in the system, [FGS]. For each boundary line, the extrapolation of $[SDS]_{eq}$ to infinitesimally small [FGS] gives an estimate for the concentration of DS^- that is in bulk solution, $[DS^-]_{bulk}$.

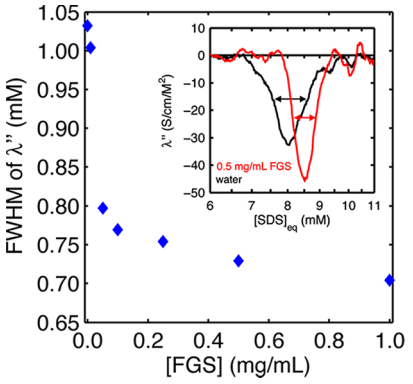

Figure 4. Full width at half-maximum (FWHM) of the peak in λ'' (second derivative of conductivity with respect to the SDS equivalent concentration, $[SDS]_{eq}$) that is indicative of the critical micelle concentration (cmc) aggregation transition, plotted as a function of the FGS suspension concentration, [FGS]. The inset shows the peaks in λ'' at the cmc transition for conductometric titrations of DI water (black) and a 0.5 mg/mL FGS suspension (red) with a 100 mM SDS solution, with the double-headed arrows indicating the FWHM.

changes in λ' were too small to detect. The values of $[SDS]_{eq}$ at the transitions between the stages are plotted in Figure 3, and a strong dependence on the concentration of FGSs in suspension, [FGS], is observed for all three. To estimate the value of $[DS^-]_{bulk}$ corresponding to each boundary line, the data in Figure 3 are extrapolated to an infinitesimally small FGS concentration (i.e., to an infinitesimally small total FGS surface area), such that $[DS^-]_{ads}$ and $[Na^+]_{ads}$ become negligible and thus $[DS^-]_{bulk}$ and $[SDS]_{eq}$ are approximately equal. Line A extrapolates to $[DS^-]_{bulk,A} = 12 \pm 5\ \mu M$, line B to $[DS^-]_{bulk,B} = 1.7 \pm 0.1$ mM, and line C to $[DS^-]_{bulk,C} = 8.0 \pm 0.1$ mM. The extrapolated $[DS^-]_{bulk}$ values are correlated to literature data for SDS in water as well as to literature data for SDS on graphite, for which $[DS^-]_{bulk}$ was measured directly, thus allowing direct comparison with our extrapolated values. Along with the framework provided by eqs 2 and 3, these correlations enable us to analyze and interpret the underlying physical processes.

We begin our analysis at higher $[SDS]_{eq}$, where surfactant behavior is much better documented than at lower $[SDS]_{eq}$. The decrease in λ' marked by line C is qualitatively similar to the decrease in λ' that is indicative of the cmc aggregation transition in the DI water titration. Indeed, the extrapolated value of $[DS^-]_{bulk,C}$ corresponds, within error, to the cmc for SDS in water that is measured herein as well as reported in the literature.[39,41,50,51] At $[SDS]_{eq}$ above this transition, the values of λ' in both the presence and absence of FGSs are within error of each other, which indicates that N is the same for both systems, as the changes in λ in this range are governed by bulk micelle formation. However, in the presence of FGS, the cmc aggregation transition is noticeably sharper than in DI water alone. To quantify this observation, the second derivative of λ with respect to $[SDS]_{eq}$ (λ'') is calculated. As shown in the inset of Figure 4 for DI water and the 0.5 mg/mL FGS suspension, during the cmc transition λ'' displays a distinct peak to negative values reflecting the strong decrease in λ'. The sharpness of the transition is measured by the FWHM of the λ'' peak, the value of which is plotted against [FGS] in the main panel of Figure 4. We see that the FWHM decreases rapidly from ~1.03 mM in DI water to ~0.77 mM at 0.1 mg/mL FGS, and continues to decrease gradually to ~0.70 mM at 1.0 mg/mL FGS. Clearly, the adsorption of SDS onto FGSs (and the amount of FGS in the system) affects the sharpness of the cmc aggregation transition in bulk solution, possibly by narrowing the bulk micelle size distribution or by causing N to increase more rapidly with $[SDS]_{eq}$;[48] however, the exact mechanism is currently under further investigation.

We propose that the decrease in λ' marked by line B at $[SDS]_{eq} \approx 2.1$ mM (Figure 2b) is indicative of an aggregation transition for SDS surface micelles on FGSs, analogous to the aggregation transition for SDS micelles in bulk solution at the cmc. Therefore, we contend that the extrapolated value of $[DS^-]_{bulk,B}$ corresponds to the csac for SDS surface micelle formation on FGSs. The csac for SDS on graphite has been reported to be ~3 mM SDS, based on experimental work with two-phase dye extraction[28] and liquid-cell AFM imaging,[27] which is higher than $[DS^-]_{bulk,B}$. This may be a result of the chemical functionalities and lattice defects on FGSs causing the onset of surface micelle formation to occur at a lower $[DS^-]_{bulk}$ than on graphite; however, it should also be noted that the techniques used to measure the adsorption of SDS on graphite do not have a high degree of sensitivity for the onset of surface micelle formation. In particular, liquid-cell AFM is not capable of detecting isolated surface micelles (due to their high mobility), and thus we view the previously reported csac values as upper limits. As $[SDS]_{eq}$ increases above the csac, λ' remains lower than in the case of DI water (Stage III in Figure 2b), indicating that SDS molecules continue to adsorb onto the FGSs. This is likely due to SDS surface micelles decreasing their spacing on FGSs, a phenomenon observed by Wanless et al. for SDS surface micelles on graphite.[27] With increasing $[SDS]_{eq}$, the surface micelle packing becomes progressively denser, and the growing energetic contribution of electrostatic repulsion between adjacent surface micelles creates an increasing energetic barrier for further SDS adsorption. As a result, the fraction of added SDS that adsorbs decreases, causing λ' to gradually increase. Eventually, the FGS surface area available for SDS adsorption becomes saturated with SDS surface micelles, and $[Na^+]_{ads}$ and $[DS^-]_{ads}$ become constant. The subsequent changes in λ and λ' as SDS is added thus reflect the titration of DI water, as shown above.

dx.doi.org/10.1021/jp403876t | J. Phys. Chem. B 2013, 117, 7950−7958

We relate the conductivity behavior observed during Stages I and II to the formation of an SDS monolayer on FGSs. We suggest that during Stage I, surfactant molecules initially adsorb sparsely on FGSs,[25] and the presence of charged DS^- molecules helps separate aggregated FGSs, resulting in an increased amount of FGS surface area exposed to bulk solution. Considering that the dissociation of acidic chemical functionalities on FGSs gives rise to the initial pH of 4.5, the newly exposed acidic groups certainly release additional hydronium ions (molar conductivity ~350 $mS{\cdot}cm^{-1}M^{-1}$). This explains why λ' initially exceeds the value observed for the titration of water, even though an equal or lower value was expected. As $[SDS]_{eq}$ is increased further in Stage I, the number density of SDS molecules adsorbed on the FGSs increases, resulting in a growing electrostatic repulsion between the negatively charged surfactant head groups. As a consequence, adsorbed surfactant molecules likely dissociate to a lesser degree to allow for denser packing,[15] similar to the decreased dissociation in bulk micelles at concentrations above the cmc,[55] and form patches of DS^- molecules that are aligned due to attractive hydrophobic and van der Waals forces between the alkyl chains.[14,15]

The adsorption of DS^- and decrease in dissociation can certainly result in λ' decreasing to values below those observed during titration of water, as can be seen in eq 3. However, the strong decrease in λ' to negative values, i.e., after λ reaches a maximum at $[SDS]_{eq} \approx 20\ \mu M$ (inset of Figure 2a), is most likely dominated by a different effect which we have not yet accounted for, namely, a counterion exchange between Na^+ and H^+: A fraction of the nondissociated SDS on FGSs substitutes the Na^+ counterion with H^+, thereby increasing the suspension pH and leaving Na^+ cations, with a smaller molar conductivity (~50 $mS{\cdot}cm^{-1}M^{-1}$), in solution. A similar phenomenon was reported by Bunton et al. for the titration of hydrochloric acid (HCl) solutions with SDS, during which a decrease in conductivity and concurrent increase in pH was observed above the cmc due to a counterion exchange between Na^+ and H^+ associating with DS^- bulk micelles.[61] Thus, we argue that if the hydronium and Na^+ ion concentrations are similar in magnitude, then the exchange of highly conducting hydronium ions with less-conducting Na^+ ions can certainly explain the appearance of a maximum in λ and subsequent negative values of λ' during Stage I. As $[SDS]_{eq}$ continues to increase beyond the concentration of hydronium ions in the system, the influence of the counterion exchange diminishes, causing λ to increase after reaching a minimum at $[SDS]_{eq} \approx 40\ \mu M$ (inset of Figure 2a) and λ' to achieve positive values.

As $[SDS]_{eq}$ increases beyond the range in which negative values of λ' are observed, SDS molecules continue to adsorb onto the FGSs and the surface coverage increases further. The increasing electrostatic repulsion between the more densely packing adsorbate creates a growing energetic barrier for further SDS adsorption, which leads to an increase in λ', since an increasing fraction of the added SDS no longer adsorbs but rather remains in the bulk solution where it is fully dissociated. This causes the conductivity to increase at a rate that approaches the value observed during the titration in the absence of FGSs. We interpret the leveling-off behavior of λ' marked by line A to be a consequence of the adsorbed monolayer having achieved full surface coverage, likely forming with surfactant molecules oriented in a head-to-head configuration and only dissociated to a small degree.[15] As $[SDS]_{eq}$ increases beyond $[DS^-]_{bulk,A}$, λ' gradually increases but remains lower than in the case of DI water (black curve, Stage II). Analogous to λ' above the csac, this behavior is indicative of surfactant molecules in the adsorbed monolayer becoming more and more densely packed. Therefore, we hypothesize that $[DS^-]_{bulk,A}$ corresponds to the bulk SDS concentration at which the adsorbed monolayer reaches full surface coverage on the FGSs but is not yet densely packed. Based on calorimetric evidence from Király et al. on the adsorption of similar surfactants on graphitic carbon,[18,19] the transition from sparsely adsorbed surfactant molecules to a densely packed monolayer (i.e., from Stage I to Stage II of the titration) most likely occurs via the coexistence of surfactant-rich and surfactant-lean regions.

The FGS surface area that is available for SDS adsorption is estimated using the slope of line C in Figure 3, which is 0.98 mmol SDS/g FGS. As discussed above, line C represents the cmc of SDS in water. At this surfactant concentration, FGSs are fully covered with SDS surface micelles. Assuming the surface micelles are hemicylindrical, and that each cross section has an aggregation number of 7 and occupies an area of ~7 nm^2,[27] the average area per adsorbed surfactant molecule is ~1 nm^2. If we multiply this value by the slope of line C and by Avogadro's number, then an overall FGS area of ~600 m^2/g is obtained, which is significantly less than the surface area reported from methylene blue adsorption onto FGSs in suspension.[2] This disparity in surface area is corroborated by a recent study showing strong evidence that SDS only adsorbs onto sp^2 hybridized regions of FGSs and not onto regions containing chemical functionalities.[33] Although the adsorption of SDS onto FGSs appears to be energetically similar to the adsorption of SDS onto graphite (as indicated by the occurrence of the csac at similar concentrations), there are most likely regions on FGSs on which SDS adsorption does not occur. Hence, the terms "full" or "dense" SDS coverage more precisely refer only to FGS regions where SDS adsorption is feasible, and the actual surface area of FGS must be higher than the 600 m^2/g value obtained assuming full coverage on pristine graphene.

CONCLUSIONS

Using conductometric surfactant titration, we measured the adsorption of SDS on FGSs with a carbon-to-oxygen ratio of ~18, at broad SDS and FGS concentration ranges. At dilute bulk SDS concentrations (<12 μM), the decrease in λ (and the corresponding negative values of λ') is evidence of a counterion exchange between hydronium ions (from the dissociation of acidic chemical functionalities on FGS) and sodium ions coadsorbing with dodecyl sulfate monomers onto FGSs. We find that, on the regions of FGS onto which SDS adsorption occurs, an adsorbed SDS monolayer reaches full coverage by a bulk SDS concentration of ~12 μM. Additionally, the csac for surface micelle formation on FGS was measured to be ~1.5 mM SDS, which is slightly lower than the csac for SDS adsorption onto graphitic carbons. This may be due in part to the chemical functionalities and lattice defects on FGSs causing the onset of surface micelle formation to occur at a lower bulk SDS concentration than on graphitic carbons, and in part to the higher sensitivity of our measurement technique. Nevertheless, the transition from monolayer adsorption to surface micelle formation appears to occur at a similar SDS concentration on FGS as on graphitic carbon, suggesting that there is little difference in the surfactant adsorption behavior on both materials. Interestingly, the presence of FGSs causes the cmc aggregation transition to become sharper (i.e., to span a

dx.doi.org/10.1021/jp403876t | J. Phys. Chem. B 2013, 117, 7950−7958

narrower concentration range); in fact, the transition becomes even sharper as the concentration of FGSs in suspension increases. Clearly, the adsorption of SDS onto FGSs affects the behavior of SDS in bulk solution during the cmc transition, and the mechanism responsible for this phenomenon is currently under further investigation. Finally, we estimate that the FGS area available for SDS adsorption is ~600 m^2/g, which is significantly less than expected for FGSs in suspension and indicates the presence of regions on FGSs on which SDS adsorption does not occur.

APPENDIX A

Validating eq 1 for the Conductivity of SDS Solutions

The textbooks of Israelachvili and Evans both provide rigorous treatments of the thermodynamics and kinetics of micelle formation.[34,35] Eq 1 describes the conductivity behavior of the SDS solution as a function of the concentrations of the individual ionic species present in the system. To express eq 1 in terms of the SDS equivalent concentration, $[SDS]_{eq}$, separate equations are necessary to describe the system below and above the cmc.

Below the cmc, $[DS^-]_{mic}$ is effectively zero, and assuming complete monomer dissociation, $[Na^+]_{bulk}$ and $[DS^-]_{bulk}$ both equal $[SDS]_{eq}$. Equation 1 can then be written as

$$\lambda = \lambda_0 + (\Lambda_0^{Na+} + \Lambda_0^{DS-})[SDS]_{eq} \quad (A1)$$

and the corresponding expression for λ'

$$\lambda' = (\Lambda_0^{Na+} + \Lambda_0^{DS-}) \quad (A2)$$

λ is a linear function of $[SDS]_{eq}$, with a slope of $(\Lambda_0^{Na+} + \Lambda_0^{DS-})$. From Figure 2, λ' is initially 69.6 $mS{\cdot}cm^{-1}M^{-1}$. By taking Λ_0^{Na+} to be 50.1 $mS{\cdot}cm^{-1}M^{-1}$,[62] eq A2 gives a value for Λ_0^{DS-} of 19.5 $mS{\cdot}cm^{-1}M^{-1}$, which matches reported literature values of 18.5 to 21.1 $mS{\cdot}cm^{-1}M^{-1}$.[63,64]

Above the cmc, $[Na^+]_{bulk}$ and $[DS^-]_{bulk}$ are effectively constant and equal to the cmc, as the formation of micelles dominates. To mitigate electrostatic repulsion between the DS^- head groups, a fraction of the Na^+ counterions remain associated, leaving micelles with a degree of dissociation β. $[DS^-]_{mic}$ can be written as $([SDS]_{eq} - cmc)$, and λ becomes

$$\lambda = \lambda_0 + (\Lambda_0^{Na+} + \Lambda_0^{DS-})\cdot cmc + \left(\Lambda_0^{Na+}\beta + \frac{\Lambda_0^{mic}}{N}\right)([SDS]_{eq} - cmc) \quad (A3)$$

and λ' can be written as

$$\lambda' = \left(\Lambda_0^{Na+}\beta + \frac{\Lambda_0^{mic}}{N}\right) \quad (A4)$$

λ is a linear function of $[SDS]_{eq}$, now with a slope of $(\Lambda_0^{Na+}\beta + (\Lambda_0^{mic}/N))$. The first term in λ' accounts for the contribution of micelle-dissociated Na^+. Here we assume that the molar conductivity (i.e., the mobility) of sodium ions screening the micelle charge is the same as the molar conductivity of sodium ions in bulk solution. This is not necessarily accurate, but a detailed assessment of the exact contribution of Na^+ located within the electrochemical double layer of micelles lies beyond the scope of this work. The second term in λ' accounts for the contribution of the ionic micelles themselves. If SDS micelles are treated as large spherical ions, the mobility of a micelle can be calculated by combining Stokes' law with the force experienced by an ion in an electrical field

$$\Lambda_0^{mic} = zuF = \frac{z^2eF}{6\pi r\eta} \quad (A5)$$

where z is the formal charge, e is the elementary charge, F is Faraday's constant, r is the hydrodynamic radius of the ion, and η is viscosity. By taking β to be 0.22 and N to be 64,[57,63,64] Λ_0^{mic} is predicted to be ~910 $mS{\cdot}cm^{-1}M^{-1}$ from eq A3. λ' above the cmc in Figure 2 was ~24.7 $mS{\cdot}cm^{-1}M^{-1}$, and from eq A4 a value of ~875 $mS{\cdot}cm^{-1}M^{-1}$ is calculated for Λ_0^{mic}. This agrees within error with the prediction and validates the conductometric titration technique.

APPENDIX B

Estimating the Contribution of SDS-Adsorbed FGSs to Conductivity

If we assume that the average FGS has an area, A, of dimensions of 500 nm by 500 nm and a thickness, d, of 1 nm, then the molar conductivity of FGSs, Λ_0^{FGS}, can be calculated by combining the drag force on a flat plate with the force experienced by an ion in an electrical field

$$\Lambda_0^{FGS} = zuF = \frac{z^2eFd}{24\eta A} \quad (A6)$$

To obtain an upper estimate for Λ_0^{FGS}, we also assume that SDS is adsorbed as hemicylindrical surface micelles with a width of 5.5 nm and an cross-sectional aggregation number of 7,[27] and a degree of dissociation of 1 (i.e., fully dissociated, though this is unlikely to be due to the electrostatic repulsion that would occur). With these assumptions, Λ_0^{FGS} is calculated from eq A6 to be ~10^5 $mS{\cdot}cm^{-1}M^{-1}$. Assuming a density of 2.2 g/cm^3 and the same spatial dimensions as above, an FGS concentration of 1 mg/mL corresponds to ~3 nM FGS. The upper-limit contribution of FGSs to λ can be estimated by multiplying Λ_0^{FGS} by the concentration of FGSs, and thus has a value of about 10^{-1} $\mu S{\cdot}cm^{-1}$.

AUTHOR INFORMATION

Corresponding Author

*E-mail: iaksay@princeton.edu. Phone: 609-258-4393.

Notes

The authors declare no competing financial interest.

ACKNOWLEDGMENTS

This work was supported by the Pacific Northwest National Laboratory (operated for the United States Department of Energy by Battelle) under grant number DE-AC05-76RL01830.

REFERENCES

(1) Schniepp, H. C.; Li, J.-L.; McAllister, M. J.; Sai, H.; Herrera-Alonso, M.; Adamson, D. H.; Prud'homme, R. K.; Car, R.; Saville, D. A.; Aksay, I. A. Functionalized Single Graphene Sheets Derived from Splitting Graphite Oxide. *J. Phys. Chem. B* **2006**, *110*, 8535−8539.

(2) McAllister, M. J.; Li, J.-L.; Adamson, D. H.; Schniepp, H. C.; Abdala, A. A.; Liu, J.; Herrera-Alonso, M.; Milius, D. L.; Car, R.; Prud'homme, R. K.; Aksay, I. A. Single Sheet Functionalized Graphene by Oxidation and Thermal Expansion of Graphite. *Chem. Mater.* **2007**, *19*, 4396−4404.

(3) Stankovich, S.; Piner, R. D.; Chen, X.; Wu, N.; Nguyen, S. T.; Ruoff, R. S. Stable Aqueous Dispersions of Graphitic Nanoplatelets via

the Reduction of Exfoliated Graphite Oxide in the Presence of Poly(Sodium 4-Styrenesulfonate). *J. Mater. Chem.* **2006**, *16*, 155−158.
(4) Wang, D.; Choi, D.; Li, J.; Yang, Z.; Nie, Z.; Kou, R.; Hu, D.; Wang, C.; Saraf, L. V.; Zhang, J.; Aksay, I. A.; Liu, J. Self-Assembled TiO_2−Graphene Hybrid Nanostructures for Enhanced Li-Ion Insertion. *ACS Nano* **2009**, *3*, 907−914.
(5) Wang, D.; Kou, R.; Choi, D.; Yang, Z.; Nie, Z.; Li, J.; Saraf, L. V.; Hu, D.; Zhang, J.; Graff, G. L.; Liu, J.; Pope, M. A.; Aksay, I. A. Ternary Self-Assembly of Ordered Metal Oxide−Graphene Nanocomposites for Electrochemical Energy Storage. *ACS Nano* **2010**, *4*, 1587−1595.
(6) Lee, H. B.; Raghu, A. V.; Yoon, K. S.; Jeong, H. M. Preparation and Characterization of Poly(Ethylene Oxide)/Graphene Nanocomposites from an Aqueous Medium. *J. Macromol. Sci., Phys.* **2010**, *49*, 802−809.
(7) Wang, J. C.; Wang, X. B.; Xu, C. H.; Zhang, M.; Shang, X. P. Preparation of Graphene/Poly(Vinyl Alcohol) Nanocomposites with Enhanced Mechanical Properties and Water Resistance. *Polym. Int.* **2011**, *60*, 816−822.
(8) Bao, C. L.; Guo, Y. Q.; Song, L.; Hu, Y. Poly(Vinyl Alcohol) Nanocomposites Based on Graphene and Graphite Oxide: A Comparative Investigation of Property and Mechanism. *J. Mater. Chem.* **2011**, *21*, 13942−13950.
(9) Korkut, S.; Roy-Mayhew, J. D.; Dabbs, D. M.; Milius, D. L.; Aksay, I. A. High Surface Area Tapes Produced with Functionalized Graphene. *ACS Nano* **2011**, *5*, 5214−5222.
(10) Fernández-Merino, M. J.; Paredes, J.; Villar-Rodil, S.; Guardia, L.; Solís-Fernández, P.; Salinas-Torres, D.; Cazorla-Amorós, D.; Morallón, E.; Martínez-Alonso, A.; Tascón, J. Investigating the Influence of Surfactants on the Stabilization of Aqueous Reduced Graphene Oxide Dispersions and the Characteristics of Their Composite Films. *Carbon* **2012**, *50*, 3184−3194.
(11) Pu, N. W.; Wang, C. A.; Liu, Y. M.; Sung, Y.; Wang, D. S.; Ger, M. D. Dispersion of Graphene in Aqueous Solutions with Different Types of Surfactants and the Production of Graphene Films by Spray or Drop Coating. *J. Taiwan Inst. Chem. Eng.* **2012**, *43*, 140−146.
(12) Aksay, I.; Trau, M.; Manne, S.; Honma, I.; Yao, N.; Zhou, L.; Fenter, P.; Eisenberger, P. Biomimetic Pathways for Assembling Inorganic Thin Films. *Science* **1996**, *273*, 892−898.
(13) Choi, K.-S.; Lichtenegger, H. C.; Stucky, G. D.; McFarland, E. W. Electrochemical Synthesis of Nanostructured ZnO Films Utilizing Self-Assembly of Surfactant Molecules at Solid-Liquid Interfaces. *J. Am. Chem. Soc.* **2002**, *124*, 12402−12403.
(14) Sammalkorpi, M.; Panagiotopoulos, A. Z.; Haataja, M. Surfactant and Hydrocarbon Aggregates on Defective Graphite Surface: Structure and Dynamics. *J. Phys. Chem. B* **2008**, *112*, 12954−12961.
(15) Tummala, N. R.; Striolo, A. Curvature Effects on the Adsorption of Aqueous Sodium-Dodecyl-Sulfate Surfactants on Carbonaceous Substrates: Structural Features and Counterion Dynamics. *Phys. Rev. E* **2009**, *80*, 021408.
(16) Tummala, N. R.; Grady, B. P.; Striolo, A. Lateral Confinement Effects on the Structural Properties of Surfactant Aggregates: SDS on Graphene. *Phys. Chem. Chem. Phys.* **2010**, *12*, 13137−13143.
(17) Hey, M. J.; MacTaggart, J. W.; Rochester, C. H. Enthalpies of Adsorption of Sodium Dodecyl Sulphate and *O*-n-Octyltetraethylene Glycol from Aqueous Solutions onto Graphitised Carbon. *J. Chem. Soc., Faraday Trans. 1* **1984**, *80*, 699−707.
(18) Király, Z.; Findenegg, G. H.; Mastalir, Á. Chain-Length Anomaly in the Two-Dimensional Ordering of the Cationic Surfactants C_nTAB at the Graphite/Water Interface, Revealed by Advanced Calorimetric Methods. *J. Phys. Chem. B* **2003**, *107*, 12492−12496.
(19) Király, Z.; Findenegg, G.; Klumpp, E.; Schlimper, H.; Dékány, I. Adsorption Calorimetric Study of the Organization of Sodium *n*-Decyl Sulfate at the Graphite/Solution Interface. *Langmuir* **2001**, *17*, 2420−2425.
(20) Zhu, B.-Y.; Gu, T. General Isotherm Equation for Adsorption of Surfactants at Solid/Liquid Interfaces. Part 1. Theoretical. *J. Chem. Soc., Faraday Trans. 1* **1989**, *85*, 3813−3817.
(21) Kawasaki, H.; Ban, K.; Maeda, H. Investigation of the Stability of Graphite Particle Dispersion and the Hemimicelle Formation Process at Graphite/Solution Interfaces Using Atomic Force Microscopy. *J. Phys. Chem. B* **2004**, *108*, 16746−16752.
(22) Manne, S.; Cleveland, J.; Gaub, H.; Stucky, G.; Hansma, P. Direct Visualization of Surfactant Hemimicelles by Force Microscopy of the Electrical Double Layer. *Langmuir* **1994**, *10*, 4409−4413.
(23) Manne, S.; Gaub, H. E. Molecular-Organization of Surfactants at Solid-Liquid Interfaces. *Science* **1995**, *270*, 1480−1482.
(24) Manne, S.; Schäffer, T.; Huo, Q.; Hansma, P.; Morse, D.; Stucky, G.; Aksay, I. Gemini Surfactants at Solid-Liquid Interfaces: Control of Interfacial Aggregate Geometry. *Langmuir* **1997**, *13*, 6382−6387.
(25) Saville, D. A.; Chun, J.; Li, J. L.; Schniepp, H. C.; Car, R.; Aksay, I. A. Orientational Order of Molecular Assemblies on Inorganic Crystals. *Phys. Rev. Lett.* **2006**, *96*, 018301.
(26) Schniepp, H. C.; Shum, H. C.; Saville, D. A.; Aksay, I. A. Orientational Order of Molecular Assemblies on Rough Surfaces. *J. Phys. Chem. C* **2008**, *112*, 14902−14906.
(27) Wanless, E. J.; Ducker, W. A. Organization of Sodium Dodecyl Sulfate at the Graphite−Solution Interface. *J. Phys. Chem.* **1996**, *100*, 3207−3214.
(28) Greenwood, F, G.; Parfitt, G, D.; Picton, N, H.; Wharton, D, G., Adsorption and Wetting Phenomena Associated with Graphon in Aqueous Surfactant Solutions. In *Adsorption from Aqueous Solution*; American Chemical Society: Washington, DC, 1968; Vol. *79*, pp 135−144.
(29) Zhu, B.-Y.; Gu, T.; Zhao, X. General Isotherm Equation for Adsorption of Surfactants at Solid/Liquid Interfaces. Part 2. Applications. *J. Chem. Soc., Faraday Trans. 1* **1989**, *85*, 3819−3824.
(30) Kudin, K. N.; Ozbas, B.; Schniepp, H. C.; Prud'homme, R. K.; Aksay, I. A.; Car, R. Raman Spectra of Graphite Oxide and Functionalized Graphene Sheets. *Nano Lett.* **2007**, *8*, 36−41.
(31) Bagri, A.; Mattevi, C.; Acik, M.; Chabal, Y. J.; Chhowalla, M.; Shenoy, V. B. Structural Evolution During the Reduction of Chemically Derived Graphene Oxide. *Nat. Chem.* **2010**, *2*, 581−587.
(32) Yang, D.; Velamakanni, A.; Bozoklu, G.; Park, S.; Stoller, M.; Piner, R. D.; Stankovich, S.; Jung, I.; Field, D. A.; Ventrice, C. A., Jr. Chemical Analysis of Graphene Oxide Films after Heat and Chemical Treatments by X-Ray Photoelectron and Micro-Raman Spectroscopy. *Carbon* **2009**, *47*, 145−152.
(33) Glover, A. J.; Adamson, D. H.; Schniepp, H. C. Charge-Driven Selective Adsorption of Sodium Dodecyl Sulfate on Graphene Oxide Visualized by Atomic Force Microscopy. *J. Phys. Chem. C* **2012**, *116*, 20080−20085.
(34) Evans, D. F.; Wennerström, H. *The Colloidal Domain: Where Physics, Chemistry, Biology, and Technology Meet*; VCH Publishers: Weinheim, 1994.
(35) Israelachvili, J. N., *Intermolecular and Surface Forces*; Elsevier Science, 2010.
(36) Rabe, J. P.; Buchholz, S. Commensurability and Mobility in 2-Dimensional Molecular Patterns on Graphite. *Science* **1991**, *253*, 424−427.
(37) Sek, S.; Chen, M.; Brosseau, C. L.; Lipkowski, J. In Situ STM Study of Potential-Driven Transitions in the Film of a Cationic Surfactant Adsorbed on a Au(111) Electrode Surface. *Langmuir* **2007**, *23*, 12529−12534.
(38) Shen, Y.-T.; Guan, L.; Zhu, X.-Y.; Zeng, Q.-D.; Wang, C. Submolecular Observation of Photosensitive Macrocycles and Their Isomerization Effects on Host−Guest Network. *J. Am. Chem. Soc.* **2009**, *131*, 6174−6180.
(39) Howell, O. R.; Robinson, H. The Electrical Conductivities of Aqueous Solutions of Sodium Dodecyl Sulphate and Sodium Hexadecyl Sulphate at Different Temperatures. *Proc. R. Soc. London, Ser. A* **1936**, *155*, 386−406.

(40) Evans, H. Alkyl Sulphates. Part I. Critical Micelle Concentrations of the Sodium Salts. *J. Chem. Soc.* **1956**, 579−586.
(41) Goddard, E.; Benson, G. Conductivity of Aqueous Solutions of Some Paraffin Chain Salts. *Can. J. Chem.* **1957**, *35*, 986−991.
(42) Parfitt, G.; Smith, A. Conductivity of Sodium Dodecyl Sulfate Solutions Below the Critical Micelle Concentration. *J. Phys. Chem.* **1962**, *66*, 942−943.
(43) Kohlrausch, F.; Holborn, L.; Diesselhorst, H. Neue Grundlagen für die Werthe der Leitvermögen von Electrolyten. *Ann. Phys. (Berlin)* **1898**, *300*, 417−455.
(44) Kohlrausch, F. W. G.; Holborn, L. F. *Das Leitvermögen der Elektrolyte, insbesondere der Lösungen*; BG Teubner, 1898.
(45) Staudenmaier, L. Verfahren zur Darstellung der Graphitsäure. *Ber. Dtsch. Chem. Ges.* **1898**, *31*, 1481−1487.
(46) Brunauer, S.; Emmett, P. H.; Teller, E. Adsorption of Gases in Multimolecular Layers. *J. Am. Chem. Soc.* **1938**, *60*, 309−319.
(47) Kendall, J. The Specific Conductivity of Pure Water in Equilibrium with Atmospheric Carbon Dioxide. *J. Am. Chem. Soc.* **1916**, *38*, 1480−1497.
(48) Floriano, M. A.; Caponetti, E.; Panagiotopoulos, A. Z. Micellization in Model Surfactant Systems. *Langmuir* **1999**, *15*, 3143−3151.
(49) Phillips, J. The Energetics of Micelle Formation. *Trans. Faraday Soc.* **1955**, *51*, 561−569.
(50) Williams, R.; Phillips, J.; Mysels, K. The Critical Micelle Concentration of Sodium Lauryl Sulphate at 25 °C. *Trans. Faraday Soc.* **1955**, *51*, 728−737.
(51) Anghel, D.; Ciocan, N. Critical Micelle Concentration (CMC) Determination with the Aid of Liquid Membrane Electrode Sensitive to Dodecyl Sulfate Anion. *Colloid Polym. Sci.* **1976**, *254*, 114−115.
(52) Wright, M. R. *An Introduction to Aqueous Electrolyte Solutions*; Wiley, 2007.
(53) Lewis, G. N.; Randall, M. The Activity Coefficient of Strong Electrolytes. *J. Am. Chem. Soc.* **1921**, *43*, 1112−1154.
(54) Burchfield, T. E.; Woolley, E. M. Model for Thermodynamics of Ionic Surfactant Solutions. 1. Osmotic and Activity Coefficients. *J. Phys. Chem.* **1984**, *88*, 2149−2155.
(55) Hayter, J.; Penfold, J. Determination of Micelle Structure and Charge by Neutron Small-Angle Scattering. *Colloid Polym. Sci.* **1983**, *261*, 1022−1030.
(56) Evans, D.; Mitchell, D.; Ninham, B. Ion Binding and Dressed Micelles. *J. Phys. Chem.* **1984**, *88*, 6344−6348.
(57) Benrraou, M.; Bales, B. L.; Zana, R. Effect of the Nature of the Counterion on the Properties of Anionic Surfactants. 1. CMC, Ionization Degree at the CMC and Aggregation Number of Micelles of Sodium, Cesium, Tetramethylammonium, Tetraethylammonium, Tetrapropylammonium, and Tetrabutylammonium Dodecyl Sulfates. *J. Phys. Chem. B* **2003**, *107*, 13432−13440.
(58) Vautier-Giongo, C.; Bales, B. L. Estimate of the Ionization Degree of Ionic Micelles Based on Krafft Temperature Measurements. *J. Phys. Chem. B* **2003**, *107*, 5398−5403.
(59) Quina, F. H.; Nassar, P. M.; Bonilha, J. B.; Bales, B. L. Growth of Sodium Dodecyl Sulfate Micelles with Detergent Concentration. *J. Phys. Chem.* **1995**, *99*, 17028−17031.
(60) Jusufi, A.; LeBard, D. N.; Levine, B. G.; Klein, M. L. Surfactant Concentration Effects on Micellar Properties. *J. Phys. Chem. B* **2012**, *116*, 987−991.
(61) Bunton, C. A.; Ohmenzetter, K.; Sepulveda, L. Binding of Hydrogen Ions to Anionic Micelles. *J. Phys. Chem.* **1977**, *81*, 2000−2004.
(62) Lide, D. R. *CRC Handbook of Chemistry and Physics*; CRC Press: Boca Raton, 2012.
(63) Moroi, Y.; Yoshida, N. A New Approach to Micellization Parameters: Its Application to Sodium Dodecyl Sulfate Micelle. *Langmuir* **1997**, *13*, 3909−3912.
(64) Nodehi, A.; Moosavian, M. A.; Haghighi, M. N.; Sadr, A. A New Method for Determination of the Adsorption Isotherm of SDS on Polystyrene Latex Particles Using Conductometric Titrations. *Chem. Eng. Technol.* **2007**, *30*, 1732−1738.